Title

Pion-Induced Radiative Corrections to Neutron β Decay

Journal

Physical Review Letters, 129(12)

ISSN

0031-9007

Authors

Cirigliano, Vincenzo

de Vries, Jordy

Hayen, Leendert

et al.

Publication Date

2022-09-16

DOI

10.1103/physrevlett.129.121801

LA-UR-21-31960
INT-PUB-22-005

Pion-induced radiative corrections to neutron beta-decay

Vincenzo Cirigliano,[1,2,*] Jordy de Vries,[3,4,†] Leendert Hayen,[5,6,‡]
Emanuele Mereghetti,[1,§] and André Walker-Loud[7,¶]

[1]*Los Alamos National Laboratory, Theoretical Division T-2, Los Alamos, NM 87545, USA*
[2]*Institute for Nuclear Theory, University of Washington, Seattle WA 98195-1550*
[3]*Institute for Theoretical Physics Amsterdam and Delta Institute for Theoretical Physics, University of Amsterdam, Science Park 904, 1098 XH Amsterdam, The Netherlands*
[4]*Nikhef, Theory Group, Science Park 105, 1098 XG, Amsterdam, The Netherlands*
[5]*Department of Physics, North Carolina State University, Raleigh, North Carolina 27695, USA*
[6]*Triangle Universities Nuclear Laboratory, Durham, North Carolina 27708, USA*
[7]*Nuclear Science Division, Lawrence Berkeley National Laboratory, Berkeley, CA 94720, USA*

We compute the electromagnetic corrections to neutron beta decay using a low-energy hadronic effective field theory. We identify and compute new radiative corrections arising from virtual pions that were missed in previous studies. The largest correction is a percent-level shift in the axial charge of the nucleon proportional to the electromagnetic part of the pion-mass splitting. Smaller corrections, comparable to anticipated experimental precision, impact the β-ν angular correlations and the β-asymmetry. We comment on implications of our results for the comparison of the experimentally measured axial charge with first-principle computations using lattice QCD and on the potential of β-decay experiments to constrain beyond-the-Standard-Model interactions.

PACS numbers:
Keywords:

Introduction — High-precision measurements of low-energy processes, such as β decays of mesons, neutron, and nuclei, probe the existence of new physics at very high energy scales through quantum fluctuations. Recent developments in the study of β decay rates at the sub-% level [1–5] have led to a 3-5σ tension with the Standard Model (SM) interpretation in terms of the unitary Cabibbo-Kobayashi-Maskawa (CKM) quark mixing matrix [5, 6]. Further, global analyses of β decay observables [7, 8] have highlighted additional avenues for β decays to probe physics beyond the Standard Model (BSM) at the multi-TeV scale, such as the comparison of the experimentally extracted weak axial charge, g_A, with precise lattice Quantum ChromoDynamics (QCD) calculations [9–11]. This test is a unique and sensitive probe of BSM right-handed charged currents.

Given the expected improvements in experimental precision in the next few years [12–14], a necessary condition to use neutron decay as probe of BSM physics is to have high-precision calculations *within the SM*, including sub-% level recoil and radiative corrections with controlled uncertainties. These prospects have spurred new theoretical activity, which has focused first on radiative corrections to the strength of the Fermi transition (vector coupling) [1–4], and more recently on the corrections to the Gamow-Teller (axial) coupling [15, 16]. These recent studies are all rooted in the current algebra approach developed in the sixties and seventies [17, 18], combined with the novel use of dispersive techniques.

In principle, lattice QCD can be used to compute the full Standard Model $n \to pe\bar{\nu}$ decay amplitude including radiative QED corrections, similar to the determination of the leptonic pion decay rate [19, 20]. However, it will be some years before these calculations reach sufficient precision. Currently, lattice QCD calculations are carried out in the isospin limit. The global average determination of g_A carries a 2.2% uncertainty [21] with one result achieving a 0.74% uncertainty [11, 22]. The PDG average value, on the other hand, has an 0.1% uncertainty [6] with the most precise experiment having an 0.035% uncertainty [23].

In this work, we perform a systematic study of neutron decay using effective field theory (EFT). We compute new structure-dependent electromagnetic corrections originating at the pion mass scale, including effects of $\mathcal{O}(\alpha)$ and $\mathcal{O}(\alpha m_\pi/m_N)$, with $\alpha = e^2/4\pi$ the fine-structure constant and $m_\pi(m_N)$ the pion (nucleon) mass. By doing so we uncover new *percent-level* electromagnetic corrections to the axial coupling g_A, which were missed both in the only other neutron β decay EFT analysis [24] and recent dispersive treatments [15, 16].

Neutron decay from the Standard Model — The energy release in neutron decay is roughly the mass splitting of the neutron and proton, i.e. $q_{\rm ext} \sim m_n - m_p \sim 1$ MeV, which is significantly smaller than the nucleon mass. The energy scale of nucleon structure corrections, on the other hand, is related to the pion mass, so that $m_N \gg m_\pi \gg m_n - m_p$. Large scale separations, such as these, make for ideal systems for an EFT description.

As a consequence, corrections to neutron β decay can be parametrized in terms of two small parameters: (*i*) $\epsilon_{\rm recoil} = q_{\rm ext}/m_N \sim 0.1\%$ which characterizes small kinetic corrections; (*ii*) $\epsilon_{\not\pi} = q_{\rm ext}/m_\pi \sim 1\%$, which characterizes nucleon structure corrections dominated by radiative pion contributions. At these relatively low energies, the decay amplitude can be described by a non-

relativistic Lagrangian density (see also Refs. [24, 25])

$$\begin{aligned}\mathcal{L}_{\not\pi} = -\sqrt{2}G_F V_{ud}\Big[&\bar{e}\gamma_\mu P_L\nu_e\Big(\bar{N}\left(g_V v_\mu - 2g_A S_\mu\right)\tau^+ N \\ &+ \frac{i}{2m_N}\bar{N}(v^\mu v^\nu - g^{\mu\nu} - 2g_A v^\mu S^\nu)(\overleftarrow{\partial} - \overrightarrow{\partial})_\nu \tau^+ N\Big) \\ &+ \frac{ic_T m_e}{m_N}\bar{N}\left(S^\mu v^\nu - S^\nu v^\mu\right)\tau^+ N\ (\bar{e}\sigma_{\mu\nu}P_L\nu) \\ &+ \frac{i\mu_{\rm weak}}{m_N}\bar{N}[S^\mu, S^\nu]\tau^+ N\,\partial_\nu\left(\bar{e}\gamma_\mu P_L\nu\right)\Big] + \dots \end{aligned} \tag{1}$$

where pions have been integrated out (hence subscript $\not\pi$), and the ellipsis denote terms not affected by our analysis. In this expression, $N^T = (p, n)$ is an isodoublet of nucleons, while v_μ and S_μ represent the velocity and spin of the nucleon, respectively. The effective vector and axial-vector couplings $g_{V,A}$ are related, as discussed below, to the isovector nucleon vector and axial charges, while $\mu_{\rm weak}$ and c_T are the weak magnetic moment and an effective tensor coupling, respectively. The Lagrangian (1) can be used to compute the differential neutron decay rate and the parameters can then be fitted to data.

There are a number of short-comings to this approach. First, by utilizing measured values of $V_{ud}\,g_V$, g_A/g_V, $\mu_{\rm weak}$, and c_T, we cannot extract fundamental SM parameters nor distinguish SM from BSM contributions to these low-energy constants (LECs). Second, it is not possible to disentangle, for example, how much of g_A arises from isospin symmetric QCD versus electromagnetic contributions. Therefore, it is desirable to utilize an EFT Lagrangian which encodes the corrections as functions of the SM parameters, such as the quark masses and the electromagnetic couplings. This is known as chiral perturbation theory (χPT) [26, 27], or specifically for baryons, heavy baryon χPT (HBχPT) [28]. The cost of such a description is the introduction of new scales, m_π and $\Lambda_\chi = 4\pi F_\pi \sim 1$ GeV with $F_\pi \simeq 92.4$ MeV, which form another expansion parameter, $\epsilon_\chi = m_\pi/\Lambda_\chi$, and new operators with potentially undetermined LECs.

Radiative corrections to neutron decay can be organized in a double expansion in $\alpha\epsilon_\chi^n\epsilon_{\not\pi}^m$. First, we integrate out the pions and match the χPT amplitude to the $\not\pi$EFT amplitude, thus determining the quark mass and electromagnetic corrections to effective couplings such as g_A. Then, the neutron decay amplitude can be computed with $\not\pi$EFT (with dynamical photons and leptons) while retaining explicit sensitivity to the parameters of the Standard Model. In our analysis of the decay amplitude we retain terms of $\mathcal{O}(G_F\epsilon_{\rm recoil})$, known in the literature, $\mathcal{O}(G_F\alpha)$, where we uncover previously overlooked effects, and terms of $\mathcal{O}(G_F\alpha\epsilon_\chi)$ and $\mathcal{O}(G_F\alpha\epsilon_{\not\pi})$, never before considered in the literature.

χPT setup for neutron decay — To study radiative corrections to weak semi-leptonic transitions, we adopt the HBχPT framework [28] with dynamical photons [29–31] and leptons, in analogy with the meson sector [32]. This EFT provides a necessary intermediate step in the analysis of neutron decay, before integrating out pions, and is the starting point for the study of related processes such as muon capture, low-energy neutrino-nucleus scattering, and nuclear β decays, which of course require a non-trivial generalization to multi-nucleon effects.

In χPT with dynamical photons and leptons, semileptonic amplitudes are expanded in the Fermi constant G_F (to first order), the electromagnetic fine structure constant α, and ϵ_χ, while keeping all orders in $q_{\rm ext}/m_\pi$, according to Weinberg's power counting [33–35]. Following standard practice, derivatives ($\partial \sim p$) and the electroweak couplings e, G_F are assigned chiral dimension one, while the light quark mass is assigned chiral dimension two ($m_\pi^2 \sim p^2$). The relevant effective Lagrangians, ordered according to their chiral dimension, are

$$\mathcal{L}_\pi = \mathcal{L}_\pi^{(2)} + \dots \tag{2a}$$
$$\mathcal{L}_{\pi N} = \mathcal{L}_{\pi N}^{(1)} + \mathcal{L}_{\pi N}^{(2)} + \mathcal{L}_{\pi N}^{(3)} + \dots \tag{2b}$$
$$\mathcal{L}_{\rm lept} \equiv \mathcal{L}_{\rm lept}^{(1)} = \bar{e}\left(i\partial\!\!\!/ + eA\!\!\!/ - m_e\right)e + \bar{\nu}i\partial\!\!\!/\nu\ . \tag{2c}$$

At a given chiral dimension, one can further separate the strong and electromagnetic Lagrangians

$$\mathcal{L}_\pi^{(2)} = \mathcal{L}_\pi^{p^2} + \mathcal{L}_\pi^{e^2p^0} \tag{3a}$$
$$\mathcal{L}_{\pi N}^{(1)} = \mathcal{L}_{\pi N}^{p} \tag{3b}$$
$$\mathcal{L}_{\pi N}^{(2)} = \mathcal{L}_{\pi N}^{p^2} + \mathcal{L}_{\pi N}^{e^2p^0} \tag{3c}$$
$$\mathcal{L}_{\pi N}^{(3)} = \mathcal{L}_{\pi N}^{p^3} + \mathcal{L}_{\pi N}^{e^2p} + \mathcal{L}_{\pi N\ell}^{e^2p}\ , \tag{3d}$$

whose explicit forms are given in the Appendix, where for the first time we present the effective Lagrangian $\mathcal{L}_{\pi N\ell}^{e^2p}$ that reabsorbs the divergences from one loop diagrams involving nucleons, photons, and charged leptons.

The leading amplitude $\mathcal{A}^{G_Fp^0}$ arises from one insertion of the lowest order Lagrangian $\mathcal{L}_{\pi N}^p$ expanded to first order in the external weak currents

$$\mathcal{L}_{\pi N}^p \supset -\sqrt{2}G_F V_{ud}\,\bar{N}\left(v_\mu - 2g_A^{(0)}S_\mu\right)\tau^+ N\ \bar{e}\gamma_\mu P_L\nu_e\ , \tag{4}$$

where $g_A^{(0)}$ denotes the nucleon axial charge in the chiral limit and in absence of electromagnetic effects.

To capture electromagnetic corrections to $\mathcal{O}(G_F\alpha)$, $\mathcal{O}(G_F\alpha\epsilon_\chi)$, and $\mathcal{O}(G_F\alpha\epsilon_{\not\pi})$, we need to compute the neutron decay amplitude to chiral dimension three ($\mathcal{A}^{e^2G_Fp^0}$) and four ($\mathcal{A}^{e^2G_Fp}$). The former arises from one-loop diagrams involving virtual nucleons, pions, photons, and charged leptons, with vertices from $\mathcal{L}_{\pi N}^p$ and $\mathcal{L}_\pi^{e^2p^0}$ (see Fig. 1, upper panel). Here, an important role is played by insertions of

$$\mathcal{L}_\pi^{e^2p^0} = 2e^2F_\pi^2Z_\pi\pi^+\pi^- + O(\pi^4), \tag{5}$$

with the LEC Z_π fixed by the relation $m^2_{\pi^\pm} - m^2_{\pi^0} = 2e^2F^2_\pi Z_\pi$, up to higher-order corrections. Additional contributions arise from tree-level graphs with one insertion of $\mathcal{L}^{e^2p}_{\pi N}$ or $\mathcal{L}^{e^2p}_{\pi N\ell}$. The $\mathcal{A}^{e^2G_Fp}$ amplitude, on the other hand, is a combination of one-loop diagrams with one vertex from $\mathcal{L}^{p^2}_{\pi N}$ or $\mathcal{L}^{e^2p^0}_{\pi N}$ and any number of vertices from $\mathcal{L}^{(1)}_{\pi N}$ and $\mathcal{L}^{(2)}_{\pi}$ (see Fig. 1, lower panel).

Matching at $\mathcal{O}(\alpha)$ and $O(\alpha\epsilon_\chi)$ – The diagrams contributing to the matching between χPT and $\not\pi$EFT at $\mathcal{O}(\epsilon^0_\chi)$ and $\mathcal{O}(\epsilon_\chi)$ are shown in Fig. 1. The result of this matching for the leading vector and axial operators is given by

$$g_{V/A} = g^{(0)}_{V/A}\left[1+\sum_{n=2}^{\infty}\Delta^{(n)}_{V/A,\chi}+\frac{\alpha}{2\pi}\sum_{n=0}^{\infty}\Delta^{(n)}_{V/A,\mathrm{em}} + \left(\frac{m_u-m_d}{\Lambda_\chi}\right)^{n_{V/A}}\sum_{n=0}^{\infty}\Delta^{(n)}_{V/A,\delta m}\right], \quad (6)$$

where $g^{(0)}_V = 1$, $\Delta^{(n)}_{\chi,\mathrm{em},\delta m} \sim O(\epsilon^n_\chi)$, and $n_A = 1$, $n_V = 2$ [36, 37]. Explicit calculation gives $\Delta^{(0),(1)}_{A,\delta m} = 0$ and we do not consider the tiny effect of $\Delta^{(0)}_{V,\delta m} \neq 0$. Concerning the chiral corrections in the isospin limit, $\Delta^{(n)}_{V,\chi}$ vanish due to conservation of the vector current, while $\Delta^{(n)}_{A,\chi}$ have been calculated up to $n = 4$ in Refs. [38–40], and can for our purposes be absorbed into a definition of g_A in the isospin limit, which we denote by g^{QCD}_A.

To $O(\alpha\epsilon^0_\chi)$ we consider the diagrams in Fig. 1, upper panel. Diagram $(a1)$ appears in the same form in both EFTs, and thus does not contribute to the matching. An explicit calculation shows that the $\mathcal{O}(\epsilon^0_{\not\pi})$ term of diagrams $(b1)$ and $(d1)$ and $(c1)$ and $(e1)$ cancels, leaving $\mathcal{O}(\epsilon_{\not\pi})$ corrections discussed below. Diagrams $(g1)$ and $(j1)$ vanish exactly at $\mathcal{O}(\epsilon^0_\chi)$, while $(f1)$, $(h1)$, $(i1)$ contribute to the vector operator only to be cancelled by corrections to the nucleon wavefunction renormalization (WFR) at $q = 0$. As a consequence, g_V does not receive loop corrections in the matching between χPT and $\not\pi$EFT, instead picking up contributions only from local operators of $\mathcal{O}(e^2p)$ so that $\Delta^{(0)}_{V,\mathrm{em}} = \hat{C}_V$. By contrast, the axial operator is modified through diagram $(i1)$, the WFR, and local operators of $O(e^2p)$, leading to

$$\Delta^{(0)}_{A,\mathrm{em}} = Z_\pi\left[\frac{1+3g^{(0)2}_A}{2}\left(\log\frac{\mu^2}{m^2_\pi}-1\right)-g^{(0)2}_A\right]+\hat{C}_A(\mu)\,. \quad (7)$$

We provide in the Appendix the explicit dependence of $\hat{C}_{V,A}$ on the LECs of $\mathcal{O}(e^2p)$. Here we note that as written, $\hat{C}_{V,A}$ contain information about short-distance physics and in particular large logarithms connecting the weak scale to the hadronic scale [41] and finite terms that have been calculated via dispersive methods [1–4].

A similar analysis applies to the NLO amplitude, for which we report a few representative diagrams in the lower panel of Fig. 1. At $q = 0$, all diagrams contributing to the vector operator are cancelled by the WFR, resulting in $\Delta^{(1)}_{V,\mathrm{em}} = 0$. We are left with a correction to g_A

$$\Delta^{(1)}_{A,\mathrm{em}} = Z_\pi\, 4\pi m_\pi\left[c_4 - c_3 + \frac{3}{8m_N} + \frac{9}{16m_N}g^{(0)2}_A\right], \quad (8)$$

dominated by the LECs $c_{3,4}$ from $\mathcal{L}^{p^2}_{\pi N}$ that contribute via topology (a2).

Matching at $\mathcal{O}(\alpha\epsilon_{\not\pi})$ — Through our final matching step, we identify additional isospin breaking terms to the LECs of the pion-less Lagrangian. Specifically, the pion loops with the vector current coupling to two pions (topology $(f1)$) induce an isospin-breaking correction to the weak magnetism term. In terms of the physical nucleon magnetic moments, $\mu_{n/p}$ (themselves containing electromagnetic shifts), we find

$$\mu_{\mathrm{weak}} - (\mu_p - \mu_n) = -\frac{\alpha Z_\pi}{2\pi}\frac{g^2_A m_N \pi}{m_\pi}\,. \quad (9)$$

which is not captured in experimental analyses thus far. Finally, the pion-γ box $(b1)$ induces the tensor coupling

$$c_T = \frac{\alpha}{2\pi}\frac{g_A m_N \pi}{3m_\pi}\,. \quad (10)$$

We discuss the numerical implications of these results below.

Connection to previous literature — Recent approaches using current algebra and dispersion techniques [15, 16] evaluated axial contributions as originating from vertex corrections, in which the virtual photon is emitted and absorbed by the hadronic line, and γW box, in which the virtual photon is exchanged between the hadronic and electron lines. The latter was found to be largely consistent with the vector contribution using experimental data of the polarized Bjorken sum rule [15] and additional nucleon scattering data [16], as such including inelastic contributions without explicit calculation. The vertex corrections, on the other hand, have only been calculated in limiting scenarios. Following the notation of Ref. [15], the *a priori* non-zero contribution depends on a three-point function

$$\mathcal{D}_\gamma = \int\frac{d^4k}{k^2}\int d^4y e^{i\bar{q}y}\int d^4x e^{ikx} \times\langle p_f|T\left\{\partial_\mu J^\mu_W(y)J^\lambda_\gamma(x)J^\gamma_\lambda(0)\right\}|p_i\rangle\,, \quad (11)$$

where $\gamma(W)$ denotes electromagnetic (weak) currents, and $T\{\ldots\}$ the time-ordered product. In the chiral limit the divergence of the weak axial current vanishes ($\partial_\mu A^\mu \propto m_\pi \to 0$), while the vector current is conserved to higher order corrections in α and $m_d - m_u$. Ref. [15]

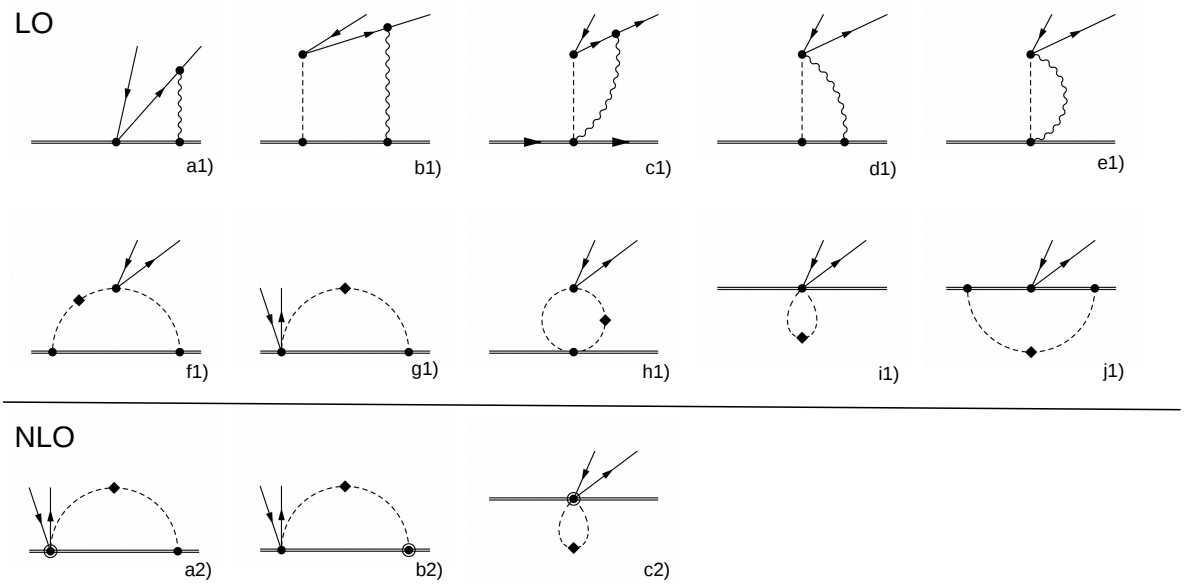

FIG. 1: Diagrams contributing to the matching between χPT and $\not$EFT at $\mathcal{O}(\epsilon_\chi^0)$ (upper panel) and $\mathcal{O}(\epsilon_\chi)$ (lower panel). Single, double, wavy, and dashed lines denote, respectively, leptons, nucleons, photons, and pions. Dots refer to interactions from the lowest-order chiral Lagrangians $\mathcal{L}_\pi^{p^2}$ and $\mathcal{L}_{\pi N}^{p}$, while diamonds represent insertions of $\mathcal{L}_\pi^{e^2p^0}$. Circled dots denote interactions from the NLO chiral Lagrangian $\mathcal{L}_{\pi N}^{p^2}$.

only considered the asymptotic and elastic contributions to Eq. (11), i.e. inserting a complete set of states in between every current and retaining only the nucleon. Assuming isospin symmetry then leads to a vanishing contribution for the three-point function [15]. Recognizing diagrams $i1, j1, a2, \ldots$ in Fig. 1 to correspond to an explicit treatment of these vertex corrections, the results presented here expand upon the simplified approach of Ref. [15] to find much larger than anticipated isospin-breaking corrections.

Numerical impact — We now estimate the numerical impact of the various corrections, starting with our main new finding, i.e., the electromagnetic shift to $\lambda = g_A/g_V$. Including BSM contributions, the relation between the experimentally extracted λ and the (isosymmetric) QCD axial charge is given by [9]

$$\lambda = g_A^{\rm QCD}\left(1 + \delta_{\rm RC}^{(\lambda)} - 2{\rm Re}(\epsilon_R)\right) , \qquad (12)$$

where $\epsilon_R \sim (246\,{\rm GeV}/\Lambda_{\rm BSM})^2$ is a BSM right-handed current contribution appearing at an energy scale $\Lambda_{\rm BSM}$ [9, 10]. To the order we are working the radiative correction is

$$\delta_{\rm RC}^{(\lambda)} = \frac{\alpha}{2\pi}\left(\Delta_{A,{\rm em}}^{(0)} + \Delta_{A,{\rm em}}^{(1)} - \Delta_{V{\rm em}}^{(0)}\right) . \qquad (13)$$

For the numerical evaluation of the loop contributions to $\Delta_{A,{\rm em}}^{(0),(1)}$ we use $Z_\pi = 0.81$ (obtained from the physical pion mass difference and $F_\pi = 92.4$ MeV) and the average nucleon mass $m_N = 938.9$ MeV. In the loops we set $g_A^{(0)} = g_A \approx 1.27$ [6], as the difference formally contributes to higher chiral order. Existing lattice data indeed indicate that g_A has a mild m_π dependence [11, 42]. The NLO LECs c_3 and c_4 have been extracted from pion-nucleon scattering [43, 44]. They show a sizable dependence on the chiral order at which the fit to π-N data is carried out, with a big change between NLO and N^{2}LO, stabilizing between N^{2}LO and N^{3}LO. For the corrections we find

$$\Delta_{A-V,{\rm em}}^{(0)} \in \{2.4,\, 5.7\}\,,\ \Delta_{A,{\rm em}}^{(1)} = \{10.0, 14.5, 15.9\}, \qquad (14)$$

where the range in $\Delta_{A-V,{\rm em}}^{(0)}$ is obtained by setting $\hat{C}_A(\mu) - \hat{C}_V = 0$ and varying μ between 0.5 and 1 GeV, while the three values of $\Delta_{A,{\rm em}}^{(1)}$ are obtained by using $c_{3,4}$ extracted to NLO, N^{2}LO, and N^{3}LO [44]. While the NLO correction is somewhat larger than the LO one, we stress that we do not know the full LO correction because we have set the counter term contribution $\hat{C}_A - \hat{C}_V$ to zero. In addition, in an EFT without explicit Δ degrees of freedom, c_3 and c_4 are dominated by Δ contributions and thus anomalously large. Combining the corrections, we estimate a correction to λ at the percent level,

$$\delta_{\rm RC}^{(\lambda)} \in \{1.4,\, 2.6\}\cdot 10^{-2}\,. \qquad (15)$$

This shift has no impact on the current first-row CKM discrepancy because the most accurate determination

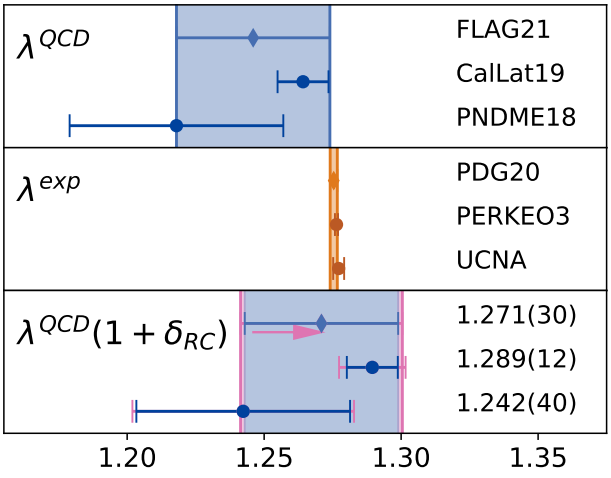

FIG. 2: Overview of the required shift to lattice QCD determinations of g_A and comparison with current experimental determination of λ. The bottom panel shows the shift and increased uncertainty in magenta with corrected values. The keys in the figure are FLAG21 [21], CalLat19 [22], PNDME18 [42], PDG21 [6], PERKEO3 [23], UCNA [45].

of λ is at present obtained from experiments, where these corrections are automatically included. The correction does have a big impact when comparing with first-principles lattice QCD computations of neutron β decay. Present lattice calculations of g_A work in the isospin limit without QED, but Eq. (15) shows these results cannot be directly compared to the experimentally extracted value of g_A without subtracting the newly identified isospin-breaking radiative corrections in this Letter.

In Fig. 2 we show the significance of the correction $\delta_{\rm RC}^{(\lambda)}$ in comparing lattice QCD calculations with the state-of-the-art experimental determination of λ. Compared to the most precise individual lattice calculation [22], our radiative corrections corresponds to a 2.7σ shift and a more modest $\sim 1\sigma$ shift in the conservative FLAG'21 average [21]. $\delta_{\rm RC}^{(\lambda)}$ generally improves the agreement between lattice QCD and experimental determination of λ and is essential if one wishes to obtain robust ranges (or constraints) on right-handed currents. For example, assuming existing central values and an increased lattice-QCD precision, the neglect of radiative corrections ($\delta_{\rm RC}^{(\lambda)}$) would wrongfully point to BSM physics at $\mathcal{O}(1\,\text{TeV})$.

Isospin-breaking corrections to the weak magnetism do translate into explicit spectral changes (see the appendix for the full differential decay rate). Relative corrections of $\mathcal{O}(10^{-4})$ occur in the SM predictions of both a, the β-ν angular correlation, and A, the β-asymmetry. These are comparable to anticipated experimental precision in the coming decade within the context of CKM unitarity tests [12]. Even larger relative changes ($\mathcal{O}(0.1\%)$) can occur due to cancellations in the leading-order SM prediction, such as in nuclear mirror systems used in complementary $|V_{ud}|$ determinations [46]. An extension of this effort to nuclear systems is deemed crucial and fits within rejuvenated superallowed efforts [5, 47]. On the other hand, the induced tensor coupling c_T produces a shift to the Fierz term and the neutrino-asymmetry parameter B at the level of 10^{-5}, negligible in light of the expected experimental accuracies.

Conclusions and outlook — By using a systematic effective field theory approach we have identified and computed novel radiative corrections to neutron β-decay. The largest correction, at the percent level, can be understood as a QED correction to the nucleon axial charge. While this does not impact the extraction of V_{ud} from experiments, it has important consequences for the potential of β-decay experiments to constrain BSM right-handed currents when comparing the measured value of $\lambda = g_A/g_V$ to the first-principles calculation of the same quantity with lattice QCD. In addition, we have identified changes in the neutron differential decay rate, in particular a shift in the β-ν angular correlation and the β-asymmetry, that are relevant for next-generation experiments.

The new shift in the nucleon axial charge depends upon non-analytic contributions associated with pion loops as well as analytic short-distance corrections parameterized by LECs. The LECs that lead to the largest part of the correction (c_3 and c_4) are precisely extracted from pion-nucleon scattering data, but others are presently unknown leading to a sizable uncertainty in our results. Lattice QCD can compute the hadronic $n \to p$ amplitude in the presence of QED [19, 20], which enables a determination of the unknown LECs. There are subtleties that must be addressed related to gauge invariance and the non-factorizable contributions to the renormalization of the four-fermion operator [48]. QED$_{\rm M}$ [49], in which the photon is given a non-zero mass, may simplify the identification of the matrix element of interest by increasing the energy gap to the excited state contamination.

Looking beyond neutron decay, it is very possible that similar-sized corrections affect nuclear β-decay. The computations in this Letter provide the first step towards a full EFT treatment of radiative corrections to the multi-nucleon level. Given the interest in these low-energy precision tests of the Standard Model and the existing deviations from first-row CKM unitarity, it is imperative to accurately determine these radiative corrections in order to make full use of the anticipated precision of upcoming experiments.

Acknowledgements.—We thank Misha Gorchtein and Martin Hoferichter for interesting conversations. The work of AWL was supported in part by the U.S. Department of Energy, Office of Science, Office of Nuclear Physics under Awards No. DE-AC02-05CH11231. EM is supported by the US Department of Energy through

the Office of Nuclear Physics and the LDRD program at Los Alamos National Laboratory. Los Alamos National Laboratory is operated by Triad National Security, LLC, for the National Nuclear Security Administration of U.S. Department of Energy (Contract No. 89233218CNA000001). JdV acknowledges support from the Dutch Research Council (NWO) in the form of a VIDI grant. L.H. acknowledges support by the U.S. National Science Foundation (Grant No. PHY-1914133), U.S. Department of Energy (Grant No. DE-FG02-ER41042)

APPENDIX

Effective Lagrangians and power counting — We start from two-flavor QCD in presence of external sources

$$\begin{aligned}\mathcal{L} &= \mathcal{L}_{\rm QCD} - \bar{q}_R(s+ip)q_L - \bar{q}_L(s-ip)q_R \\ &+ \bar{q}_L\gamma^\mu l_\mu q_L + \bar{q}_R\gamma^\mu r_\mu q_R \end{aligned} \tag{16}$$

where $q^T=(u,d)$ and $s(x), p(x), l_\mu(x), r_\mu(x)$ can be written in terms of quark mass, Standard Model gauge fields, and external classical fields $\bar{s}, \bar{p}, \bar{l}_\mu, \bar{r}_\mu$ as follows

$$\chi \equiv B_0(s+ip) = B_0(m_q+\bar{s}+i\bar{p}) \tag{17a}$$
$$l_\mu = -eQ_L^{EM}A_\mu + Q_L^W J_\mu^{\rm lept} + Q_L^{W\dagger}J_\mu^{\rm lept\dagger} + \bar{l}_\mu \tag{17b}$$
$$r_\mu = -eQ_R^{EM}A_\mu + \bar{r}_\mu \ . \tag{17c}$$

Here B_0 is a constant with dimension of mass, m_q is the quark mass matrix, $Q_L^{EM} = Q_R^{EM} = {\rm diag}(q_u, q_d)$ (with $q_u = 2/3, q_d = -1/3$), $Q_L^W = -2\sqrt{2}G_F V_{ud}\,\tau^+$, and $J_\mu^{\rm lept} = \bar{e}_L\gamma_\mu\nu_{eL}$. The Lagrangian in (16) is invariant under local $G = SU(2)_L \times SU(2)_R \times U(1)_V$ transformations

$$q_L \to L(x)e^{\alpha_V(x)}q_L \ , \quad q_R \to R(x)e^{\alpha_V(x)}q_R \ , \tag{18}$$

with $L, R \in SU(2)_{L,R}$, provided $Q_{L,R}^{EM}$ and Q_L^W transform as "spurions" under the chiral group $Q_L^{EM,W} \to LQ_L^{EM,W}L^\dagger$ and $Q_R^{EM} \to RQ_R^{EM}R^\dagger$, and that $\bar{l}_\mu$ and $\bar{r}_\mu$ transform as gauge fields under G. This implies

$$\chi \to R\chi L^\dagger \tag{19a}$$
$$l_\mu \to Ll_\mu L^\dagger + iL\partial_\mu L^\dagger + \partial_\mu\alpha_V \tag{19b}$$
$$r_\mu \to Rr_\mu R^\dagger + iR\partial_\mu R^\dagger + \partial_\mu\alpha_V \ . \tag{19c}$$

Note that the external sources can be decomposed in $SU(2)$ singlet and non-singlet components as follows: $l_\mu = l_\mu^{ns} + l_\mu^s$, $r_\mu = r_\mu^{ns} + r_\mu^s$.

To construct the effective chiral Lagrangians, one introduces the nucleon and pion fields as follows [50, 51],

$$N = \begin{pmatrix} p \\ n \end{pmatrix}, \ U = u^2 = e^{i\Pi/(F)}, \ \Pi = \begin{pmatrix} \pi^0 & \sqrt{2}\pi^+ \\ \sqrt{2}\pi^- & -\pi^0 \end{pmatrix} \tag{20}$$

and $F \sim F_\pi = 92.4$ MeV. These fields transform under the chiral group as follows

$$u \to LuK^\dagger(u) = K(u)uR^\dagger \tag{21a}$$
$$U \to LUR^\dagger \tag{21b}$$
$$N \to e^{3i\alpha_V}K(u)N \tag{21c}$$

where $K(u)$ is a pion-dependent $SU(2)_V$ transformation.

To construct chiral invariant Lagrangians, it is very useful to use chiral-covariant derivatives

$$D_\mu U \equiv \partial_\mu U - il_\mu U + iUr_\mu \to L(D_\mu U)R^\dagger \tag{22a}$$
$$\nabla_\mu N \equiv \left(\partial_\mu + \Gamma_\mu - i\frac{3(l_\mu^s + r_\mu^s)}{2}\right)N \to K(\nabla_\mu N) \tag{22b}$$
$$\begin{aligned}\Gamma_\mu &= \frac{1}{2}\left[u(\partial_\mu - ir_\mu^{ns})u^\dagger + u^\dagger(\partial_\mu - il_\mu^{ns})u\right] \\ &\to K(u)\Gamma_\mu K(u)^\dagger + K(u)\partial_\mu K(u)^\dagger \ . \end{aligned} \tag{22c}$$

It is also very useful to use combinations of fields that transform homogeneously with $K(u)$:

$$\begin{aligned}u_\mu &= i\left[u(\partial_\mu - ir_\mu)u^\dagger - u^\dagger(\partial_\mu - il_\mu)u\right] \\ &\to K(u)u_\mu K(u)^\dagger \end{aligned} \tag{23a}$$
$$\chi_\pm = u^\dagger\chi u^\dagger \pm u\chi^\dagger u \to K(u)\chi_\pm K(u)^\dagger \tag{23b}$$
$$\mathcal{Q}_L^{EM,W} = u^\dagger Q_L^{EM,W}u \to K(u)\mathcal{Q}_L^{EM,W}K(u)^\dagger \tag{23c}$$
$$\mathcal{Q}_R^{EM} = uQ_R^{EM}u^\dagger \to K(u)\mathcal{Q}_R^{EM}K(u)^\dagger \tag{23d}$$

Finally, in the literature one often finds the combinations of charge building blocks with definite parity

$$\mathcal{Q}_\pm \equiv \frac{1}{2}\left(\mathcal{Q}_L \pm \mathcal{Q}_R\right) \ . \tag{24}$$

The standard χPT power counting assumes that external momenta and meson masses are comparable ($q_{\rm ext} \sim m_\pi$). Including charged lepton masses one assumes $p \sim q_{\rm ext} \sim m_\mu \sim m_\pi \ll \Lambda_\chi \sim 4\pi F_\pi \sim m_N$. Given this, one makes the following assignments:

$$\partial \sim p \ , \quad \chi_\pm \sim B_0 m_q \sim m_\pi^2 \sim p^2 \ . \quad l_\mu, r_\mu \sim p \ , \tag{25}$$

with the latter identification implying $e \sim p$ and $G_F \sim p$ (though we will never go beyond one insertion of G_F and two insertions of the electromagnetic coupling e). The above scalings allow us to assign chiral dimension to each lagrangian vertex in a straightforward way.

The pion Lagrangian has the usual expansion in even chiral powers:

$$\mathcal{L}_\pi = \mathcal{L}_\pi^{(2)} + \mathcal{L}_\pi^{(4)} + ... \tag{26a}$$
$$\begin{aligned}\mathcal{L}_\pi^{(2)} &= \mathcal{L}_\pi^{p^2} + \mathcal{L}_\pi^{e^2p^0} \\ &= \frac{F^2}{4}\langle u_\mu u^\mu + \chi_+\rangle + e^2Z_\pi F^4\langle\mathcal{Q}_L^{EM}\mathcal{Q}_R^{EM}\rangle, \end{aligned} \tag{26b}$$

which leads to the identification

$$m_{\pi^\pm}^2 - m_{\pi^0}^2 = 2e^2F_\pi^2Z_\pi \ . \tag{27}$$

The gauge-kinetic leptonic Lagrangian has chiral dimension $n = 1$:

$$\mathcal{L}_{\rm lept} = \bar{e}\left(i\partial\!\!\!/ + eA\!\!\!/ - m_e\right) e + \bar{\nu} i\partial\!\!\!/ \nu \ . \tag{28}$$

To the order we work, we need to include the following purely leptonic counter-term [32]

$$\mathcal{L}^{CT}_{\rm lept} = e^2 X_6 \ \bar{e}\left(i\partial\!\!\!/ + eA\!\!\!/\right) e \ . \tag{29}$$

The pion-nucleon Lagrangian has both odd and even chiral powers, starting at $n = 1$:

$$\begin{aligned}
\mathcal{L}_{\pi N} &= \mathcal{L}^{(1)}_{\pi N} + \mathcal{L}^{(2)}_{\pi N} + \mathcal{L}^{(3)}_{\pi N} + ... && \text{(30a)}\\
\mathcal{L}^{(1)}_{\pi N} &= \mathcal{L}^{p}_{\pi N} = \bar{N}_v iv\cdot\nabla N_v + g_A \bar{N}_v S\cdot u N_v && \text{(30b)}\\
\mathcal{L}^{(2)}_{\pi N} &= \mathcal{L}^{p^2}_{\pi N} + \mathcal{L}^{e^2 p^0}_{\pi N} && \text{(30c)}\\
\mathcal{L}^{(3)}_{\pi N} &= \mathcal{L}^{p^3}_{\pi N} + \mathcal{L}^{e^2 p}_{\pi N} + \mathcal{L}^{e^2 p}_{\pi N \ell} && \text{(30d)}
\end{aligned}$$

where in the nucleon rest-frame $v^\mu = (1, \mathbf{0})$ and $S^\mu = (0, \boldsymbol{\sigma}/2)$. We have displayed explicitly here only the leading order Lagrangians and we will report below the appropriate higher order terms as needed. All these effective Lagrangian are know in the literature, see for example Ref. [31], except for $\mathcal{L}^{e^2 p}_{\pi N \ell}$, which is needed to reabsorb divergences from loops that involve virtual baryons, pions, leptons, and photons. We report here only the terms that play a significant role in our analysis.

The one-loop diagrams with virtual nucleons, pions, and photons generate divergences which are absorbed by counterterms in the $\mathcal{L}^{e^2 p}_{\pi N}$ Lagrangian. When constructing the baryon electromagnetic Lagrangian, it has been common practice in the literature [29–31] to use charge spurions corresponding to the nucleon charge matrix $\bar{Q} = diag(1, 0)$. Now $\bar{Q}$ differs from the quark charge matrix only in its $SU(2)$ singlet component: therefore the two objects have the same transformation properties under the chiral group and this procedure is justified. In what follows we indicate all the chiral building blocks built from the nucleon charge matrix with a bar. A minimal version of $\mathcal{L}^{e^2 p}_{\pi N}$ was constructed in Ref. [31]

$$\mathcal{L}^{e^2 p}_{\pi N} = e^2 \sum_{i=1,12} g_i \ \bar{N}_v \, O_i^{e^2 p} \, N_v \ , \tag{31}$$

Only four operators contribute to neutron decay at tree level,

$$\begin{aligned}
O_1^{e^2 p} &= \langle \bar{\mathcal{Q}}_+^2 - \bar{\mathcal{Q}}_-^2 \rangle \, S\cdot u && \text{(32a)}\\
O_2^{e^2 p} &= \langle \bar{\mathcal{Q}}_+ \rangle^2 \, S\cdot u && \text{(32b)}\\
O_9^{e^2 p} &= \frac{i}{2}[\bar{\mathcal{Q}}_+, v\cdot c^+] + \text{h.c.} && \text{(32c)}\\
O_{11}^{e^2 p} &= \frac{i}{2}[\bar{\mathcal{Q}}_+, S\cdot c^-] \ , && \text{(32d)}
\end{aligned}$$

with

$$c^\pm_\mu = -\frac{i}{2}\left(u[l_\mu, \bar{Q}]u^\dagger \pm u^\dagger[r_\mu, \bar{Q}]u\right) \ . \tag{33}$$

As standard practice in χPT, the divergences are subtracted as follows [26]:

$$\begin{aligned}
g_i &= \eta_i \ \lambda(\mu) + g_i^r(\mu) \ , \\
\lambda(\mu) &= \frac{\mu^{d-4}}{(4\pi)^2}\left(\frac{1}{d-4} - \frac{1}{2}\left(-\gamma + \log 4\pi + 1\right)\right) .
\end{aligned} \tag{34}$$

We use the same subtraction scheme for all LECs. The coefficients η_i can be found in Table 5 of Ref. [31]. We checked that the g_i couplings absorb correctly the divergences of diagrams without virtual leptons, thus providing a consistency check on our calculation.

The one-loop diagrams with virtual nucleons, pions, photons, and charged leptons generate divergences which are absorbed by counterterms in the new $\mathcal{L}^{e^2 p}_{\pi N \ell}$ Lagrangian. These are the analogue of the operators introduced in the meson sector in Ref. [32], that contribute to (semi)leptonic meson decays to $O(e^2 p^2)$. We find five structures, of which only the first three contribute to neutron decay at tree level

$$\mathcal{L}^{e^2 p}_{\pi N \ell} = e^2 \sum_{i=1,5} \tilde{X}_i \, \tilde{O}_i \ , \tag{35}$$

where

$$\begin{aligned}
\tilde{O}_1 &= \bar{e}\gamma_\alpha \nu_L \ \bar{N}_v v^\alpha \mathcal{Q}_L^W N_v && \text{(36a)}\\
\tilde{O}_2 &= \bar{e}\gamma_\alpha \nu_L \ \bar{N}_v v^\alpha [\mathcal{Q}_L^W, \bar{\mathcal{Q}}_R^{EM}] N_v && \text{(36b)}\\
\tilde{O}_3 &= \bar{e}\gamma_\alpha \nu_L \ \bar{N}_v S^\alpha [\mathcal{Q}_L^W, \bar{\mathcal{Q}}_R^{EM}] N_v && \text{(36c)}\\
\tilde{O}_4 &= \bar{e}\gamma_\alpha \nu_L \ \bar{N}_v v^\alpha \langle \mathcal{Q}_L^W \bar{\mathcal{Q}}_R^{EM} \rangle N_v && \text{(36d)}\\
\tilde{O}_5 &= \bar{e}\gamma_\alpha \nu_L \ \bar{N}_v S^\alpha \langle \mathcal{Q}_L^W \bar{\mathcal{Q}}_R^{EM} \rangle N_v \ . && \text{(36e)}
\end{aligned}$$

The couplings $\tilde{X}_i$ are dimensionless (note that $\mathcal{Q}_W$ carries dimension via the G_F factor).

To compute the neutron decay amplitude to $O(G_F \alpha \epsilon_\chi)$ we must consider one-loop diagrams with insertions of $\mathcal{L}^{p^2}_{\pi N}$, for which (in the notation of Ref. [52]) we use

$$\mathcal{L}^{p^2}_{\pi N} = \bar{N}\Bigg[\frac{1}{2m_N}\left((v\cdot\mathcal{D})^2-\mathcal{D}^2\right)-i\frac{g_A}{2m_N}\left\{S\cdot\mathcal{D},v\cdot u\right\}+c_1\mathrm{Tr}(\chi_+)+\left(c_2-\frac{g_A^2}{8m_N}\right)(v\cdot u)^2$$
$$+c_3 u\cdot u+\left(c_4+\frac{1}{4m_N}\right)\left[S^\mu,S^\nu\right]u_\mu u_\nu+c_5\tilde{\chi}_+-\frac{i}{4m_N}\left[S^\mu,S^\nu\right]\left((1+\kappa_1)f^+_{\mu\nu}+\frac{1}{2}(\kappa_0-\kappa_1)\mathrm{Tr}\left(f^+_{\mu\nu}\right)\right)\Bigg]N. \quad (37)$$

Given these Lagrangians, Weinberg's power counting argument [33–35] implies that connected diagrams scale as $\mathcal{A}\sim p^\nu$ with

$$\nu = 2L+1+\sum_{n=2,4,\ldots}(n-2)N_n^M+\sum_{m=1,2,\ldots}(m-1)N_m^F \quad (38)$$

where L is the number of loops and N_n^M (N_m^F) is the number of mesonic (fermionic) vertices with chiral dimension n (m). In deriving this formula, pion propagators are counted as p^{-2} and baryon / lepton propagators are counted as p^{-1}.

Using this power counting one sees that the amplitude for neutron decay can be organized as follows

$$\mathcal{A} = \mathcal{A}^{(1)}+\mathcal{A}^{(2)}+\mathcal{A}^{(3)}+\mathcal{A}^{(4)}+\ldots \quad (39a)$$
$$\mathcal{A}^{(1)} = \mathcal{A}^{G_F p^0} \quad (39b)$$
$$\mathcal{A}^{(2)} = \mathcal{A}^{G_F p} \quad (39c)$$
$$\mathcal{A}^{(3)} = \mathcal{A}^{G_F p^2}+\mathcal{A}^{e^2 G_F p^0} \quad (39d)$$
$$\mathcal{A}^{(4)} = \mathcal{A}^{G_F p^3}+\mathcal{A}^{e^2 G_F p} \quad (39e)$$
$$\ldots$$

We are interested in computing the leading and next-to-leading electromagnatic corrections to the neutron decay, which appear at chiral order $n=3$ and $n=4$, respectively. Using Eq. (38) one can easily identify the tree-level and one-loop diagrams that contribute to a given order, up to $\mathcal{A}^{(4)}$:

- The amplitude $\mathcal{A}^{(1)}$ is given by a tree-level diagram with insertion of the weak vertices from $\mathcal{L}^{(1)}_{\pi N}$.
- The amplitude $\mathcal{A}^{(2)}$ is obtained by tree-level graphs with one insertion of $\mathcal{L}^{(2)}_{\pi N}$ and any number of insertions from $\mathcal{L}^{(1)}_{\pi N}$ and $\mathcal{L}^{(2)}_{\pi}$. It contributes to neutron decay at order $G_F\epsilon_{\rm recoil}$.
- The amplitude $\mathcal{A}^{(3)}$ is given by tree-level graphs with one insertion of $\mathcal{L}^{(3)}_{\pi N}$ and any number of insertions from $\mathcal{L}^{(1)}_{\pi N}$ and $\mathcal{L}^{(2)}_{\pi}$; and by one-loop diagrams with vertices from $\mathcal{L}^{(1)}_{\pi N}$ and $\mathcal{L}^{(2)}_{\pi}$. In Fig. 1 (upper panel) we show all one-loop topologies contributing up to $O(e^2G_Fp^0)$, These involve virtual pions, virtual photons, and virtual charged leptons.
- The amplitude $\mathcal{A}^{(4)}$ is given by tree-level graphs with one insertion of $\mathcal{L}^{(4)}_{\pi N}$ and any number of insertions from $\mathcal{L}^{(1)}_{\pi N}$ and $\mathcal{L}^{(2)}_{\pi}$; and by one-loop diagrams with one vertex from $\mathcal{L}^{(2)}_{\pi N}$ and any number of vertices from $\mathcal{L}^{(1)}_{\pi N}$ and $\mathcal{L}^{(2)}_{\pi}$. Note that tree level graphs with insertion of $\mathcal{L}^{(e^2p^2)}_{\pi N}$ do not contribute. In Fig. 1 (lower panel) we show representative one-loop diagrams contributing up to $O(e^2G_Fp)$, These involve virtual pions, virtual photons, and virtual charged leptons.

The counterterm contributions to the amplitude at $O(e^2G_Fp^0)$ are captured by the combinations $\hat{C}_{V/A}$ (see Eq. (7)) as follows:

$$\hat{C}_A = 8\pi^2\left[-\frac{X_6}{2}+\frac{1}{g_A^{(0)}}\left[\tilde{X}_3+\left(g_1+g_2+\frac{g_{11}}{2}\right)\right]\right]$$
$$\hat{C}_V = 8\pi^2\left[-\frac{X_6}{2}+2\left(\tilde{X}_1-\tilde{X}_2\right)+g_9\right]. \quad (40)$$

Neutron decay rate — We now present the neutron differential decay rate up-to-and-including $\mathcal{O}(G_F\epsilon_{\rm recoil}$, $\mathcal{O}(G_F\alpha)$, $\mathcal{O}(G_F\alpha\epsilon_\chi)$, and $\mathcal{O}(G_F\alpha\epsilon_\not{\pi})$ corrections. We follow Refs. [9, 24, 53] and write

$$\frac{d\Gamma}{dE_e d\Omega_e d\Omega_\nu} = \frac{(G_F V_{ud})^2}{(2\pi)^5}(1+3\lambda^2)w(E_e)D(E_e,\vec{p}_e,\vec{p}_\nu,\vec{\sigma}_n), \quad (41)$$

where $\vec{\sigma}_n$ denotes the neutron polarization and $\lambda = g_A/g_V$. The spectrum of the electron is described by

$$w = |\vec{p}_e|E_e(E_0-E_e)^2F(E_e)\left(1+\frac{\alpha}{2\pi}\delta^{(1)}_\alpha(E_e)\right), \quad (42)$$

where $E_0=(m_n^2-m_p^2+m_e^2)/(2m_n)$ is the maximal electron energy, and $F(E_e)$ is the Fermi function for an electron in the field of the final-state proton. The radiative correction $\delta^{(1)}_\alpha$ is discussed below. The function D can

be parametrized[1] as

$$
\begin{aligned}
D &= 1 + c_0 + c_1 \frac{E_e}{m_N} + \frac{m_e}{E_e}\bar{b} + \bar{a}\frac{\vec{p}_e\cdot\vec{p}_\nu}{E_e E_\nu} + \bar{A}\frac{\vec{\sigma}\cdot\vec{p}_e}{E_e} \\
&\quad + \bar{B}\frac{\vec{\sigma}\cdot\vec{p}_\nu}{E_\nu} + \bar{C}_{aa}\left(\frac{\vec{p}_e\cdot\vec{p}_\nu}{E_e E_\nu}\right)^2 \\
&\quad + \bar{C}_{aA}\frac{\vec{p}_e\cdot\vec{p}_\nu}{E_e E_\nu}\frac{\vec{\sigma}\cdot\vec{p}_e}{E_e} + \bar{C}_{aB}\frac{\vec{p}_e\cdot\vec{p}_\nu}{E_e E_\nu}\frac{\vec{\sigma}\cdot\vec{p}_\nu}{E_\nu}\,. \qquad (43)
\end{aligned}
$$

The various coefficients can be further decomposed through [9, 53]

$$
\begin{aligned}
\bar{a} &= \left(a_{\rm LO} + c_0^{(a)} + c_1^{(a)}\frac{E_e}{m_N}\right)\left(1 + \frac{\alpha}{2\pi}\delta_\alpha^{(2)}(E_e)\right), \\
\bar{A} &= \left(A_{\rm LO} + c_0^{(A)} + c_1^{(A)}\frac{E_e}{m_N}\right)\left(1 + \frac{\alpha}{2\pi}\delta_\alpha^{(2)}(E_e)\right), \\
\bar{B} &= B_{\rm LO} + c_0^{(B)} + c_1^{(B)}\frac{E_e}{m_N} + \frac{m_e}{E_e}b_\nu\,, \\
\bar{C}_{aa} &= c_1^{(aa)}\frac{E_e}{m_N}\,, \\
\bar{C}_{aA} &= c_1^{(aA)}\frac{E_e}{m_N}\,, \\
\bar{C}_{aB} &= c_0^{(aB)} + c_1^{(aB)}\frac{E_e}{m_N}\,. \qquad (44)
\end{aligned}
$$

The LO coefficients are well known and given by

$$
\begin{aligned}
a_{\rm LO} &= \frac{1-\lambda^2}{1+3\lambda^2}\,, \\
A_{\rm LO} &= \frac{2\lambda - 2\lambda^2}{1+3\lambda^2}\,, \\
B_{\rm LO} &= \frac{2\lambda + 2\lambda^2}{1+3\lambda^2}\,. \qquad (45)
\end{aligned}
$$

We write the remaining coefficients in terms of $\bar{\mu}_V = \mu_p - \mu_n - \frac{\alpha Z_\pi}{2\pi}\frac{g_A^2 m_N \pi}{m_\pi}$ and $c_T = \frac{\alpha}{2\pi}\frac{g_A m_N \pi}{3m_\pi}$

$$
\begin{aligned}
\bar{b} &= -\frac{m_e}{m_N}\frac{1 + 2\lambda(\bar{\mu}_V + 3c_T) + \lambda^2}{1+3\lambda^2}\,, \\
c_0 &= -\frac{E_0}{m_N}\frac{2\lambda(\lambda+\bar{\mu}_V)}{1+3\lambda^2}\,, \\
c_1 &= \frac{3 + 4\lambda\bar{\mu}_V + 9\lambda^2}{1+3\lambda^2}\,, \\
c_0^{(a)} &= \frac{E_0}{m_N}\frac{2\lambda(\lambda+\bar{\mu}_V)}{1+3\lambda^2}\,, \\
c_1^{(a)} &= -\frac{4\lambda(3\lambda+\bar{\mu}_V)}{1+3\lambda^2}\,, \\
c_0^{(A)} &= \frac{E_0}{m_N}\frac{(\lambda-1)(\lambda+\bar{\mu}_V)}{1+3\lambda^2}\,, \\
c_1^{(A)} &= \frac{\lambda(7-5\lambda) + \bar{\mu}_V(1-3\lambda)}{1+3\lambda^2}\,, \\
c_0^{(B)} &= -\frac{E_0}{m_N}\frac{2\lambda(\lambda+\bar{\mu}_V)}{1+3\lambda^2}\,, \\
c_1^{(B)} &= \frac{\lambda(7+5\lambda) + \bar{\mu}_V(1+3\lambda)}{1+3\lambda^2}\,, \\
b_\nu &= -\frac{m_e}{m_N}\frac{(1+\lambda)(\lambda+\bar{\mu}_V) + 2c_T(1+2\lambda)}{1+3\lambda^2}\,, \\
c_1^{(aa)} &= -\frac{3(1-\lambda^2)}{1+3\lambda^2}\,, \\
c_1^{(aA)} &= \frac{(\lambda-1)(5\lambda+\bar{\mu}_V)}{1+3\lambda^2}\,, \\
c_0^{(aB)} &= \frac{E_0}{m_N}\frac{(1+\lambda)(\lambda+\bar{\mu}_V)}{1+3\lambda^2}\,, \\
c_1^{(aB)} &= -\frac{(1+\lambda)(7\lambda+\bar{\mu}_V)}{1+3\lambda^2}\,. \qquad (46)
\end{aligned}
$$

The explicit expressions for the radiative corrections $\delta_\alpha^{(1)}$ and $\delta_\alpha^{(2)}$ are given by

$$
\begin{aligned}
\delta_\alpha^{(1)} &= 2\hat{C}_V + 3\log\frac{\mu}{m_e} + \frac{1}{2} \\
&\quad + \frac{1+\beta^2}{\beta}\log\frac{1+\beta}{1-\beta} + \frac{1}{12\beta}\left(\frac{\bar{E}}{E_e}\right)^2\log\frac{1+\beta}{1-\beta} \\
&\quad + 4\left[\frac{1}{2\beta}\log\frac{1+\beta}{1-\beta} - 1\right]\left[\log\frac{2\bar{E}}{m_e} - \frac{3}{2} + \frac{\bar{E}}{3E_e}\right] \\
&\quad + \frac{1}{\beta}\left[-4\,{\rm Li}_2\left(\frac{2\beta}{1+\beta}\right) - \log^2\left(\frac{1+\beta}{1-\beta}\right)\right], \qquad (47) \\
\delta_\alpha^{(2)} &= \frac{1-\beta^2}{\beta}\log\frac{1+\beta}{1-\beta} \\
&\quad + \frac{4(1-\beta^2)}{3\beta^2}\frac{\bar{E}}{E_e}\left[\frac{1}{2\beta}\log\frac{1+\beta}{1-\beta} - 1\right] \\
&\quad + \frac{1}{6\beta^2}\frac{\bar{E}^2}{E_e^2}\left[\frac{1-\beta^2}{2\beta}\log\frac{1+\beta}{1-\beta} - 1\right], \qquad (48)
\end{aligned}
$$

where $\beta = |\vec{p}_e|/E_e$ and $\bar{E} = E_0 - E_e$. Our expression for $\delta_\alpha^{(1)}$ coincides with the combination of $\delta_\alpha^{(1)} + e_V^R(\mu)$ in Ref. [24] upon identifying $2\hat{C}_V$ with the combination of

[1] A possible correction to the time-reversal-odd D coefficient only enters at $\mathcal{O}(G_F\alpha\epsilon_{\rm recoil})$ [54].

counterterms $e_V - (e_1 + e_2)/2$] in Ref. [24]. Finally, expressing $\delta_\alpha^{(1)}$ in terms of the Sirlin function $g(E_e, E_0)$ [17], we find

$$\delta_\alpha^{(1)} = 2\hat{C}_V + \frac{5}{4} + 3\log\frac{\mu}{m_p} + g(E_e, E_0)\,. \qquad (49)$$

* Electronic address: cirigliano@lanl.gov
† Electronic address: j.devries4@uva.nl
‡ Electronic address: lmhayen@ncsu.edu
§ Electronic address: emereghetti@lanl.gov
¶ Electronic address: walkloud@lbl.gov

[1] C.-Y. Seng, M. Gorchtein, H. H. Patel, and M. J. Ramsey-Musolf, Phys. Rev. Lett. **121**, 241804 (2018), arXiv:1807.10197 [hep-ph] .
[2] C. Y. Seng, M. Gorchtein, and M. J. Ramsey-Musolf, Phys. Rev. D **100**, 013001 (2019), arXiv:1812.03352 [nucl-th] .
[3] A. Czarnecki, W. J. Marciano, and A. Sirlin, Phys. Rev. D **100**, 073008 (2019), arXiv:1907.06737 [hep-ph] .
[4] K. Shiells, P. G. Blunden, and W. Melnitchouk, Phys. Rev. D **104**, 033003 (2021), arXiv:2012.01580 [hep-ph] .
[5] J. Hardy and I. Towner, Phys. Rev. C **102**, 045501 (2020).
[6] P. A. Zyla et al. (Particle Data Group), PTEP **2020**, 083C01 (2020).
[7] A. Falkowski, M. González-Alonso, and O. Naviliat-Cuncic, (2020), arXiv:2010.13797 [hep-ph] .
[8] M. González-Alonso, O. Naviliat-Cuncic, and N. Severijns, Prog. Part. Nucl. Phys. **104**, 165 (2019), arXiv:1803.08732 [hep-ph] .
[9] T. Bhattacharya, V. Cirigliano, S. D. Cohen, A. Filipuzzi, M. Gonzalez-Alonso, M. L. Graesser, R. Gupta, and H.-W. Lin, Phys. Rev. D **85**, 054512 (2012), arXiv:1110.6448 [hep-ph] .
[10] S. Alioli, V. Cirigliano, W. Dekens, J. de Vries, and E. Mereghetti, JHEP **05**, 086 (2017), arXiv:1703.04751 [hep-ph] .
[11] C. Chang et al., Nature **558**, 91 (2018), arXiv:1805.12130 [hep-lat] .
[12] V. Cirigliano, A. Garcia, D. Gazit, O. Naviliat-Cuncic, G. Savard, and A. Young, (2019), arXiv:1907.02164 [nucl-ex] .
[13] D. Počanić, R. Alarcon, L. P. Alonzi, S. Baeßler, S. Balascuta, J. D. Bowman, M. A. Bychkov, J. Byrne, J. R. Calarco, V. Cianciolo, C. Crawford, E. Frlež, M. T. Gericke, G. L. Greene, R. K. Grzywacz, V. Gudkov, F. W. Hersman, A. Klein, J. Martin, S. A. Page, A. Palladino, S. I. Penttilä, K. P. Rykaczewski, W. S. Wilburn, A. R. Young, and G. R. Young, Nuclear Instruments and Methods in Physics Research, Section A: Accelerators, Spectrometers, Detectors and Associated Equipment **611**, 211 (2009).
[14] D. Dubbers, H. Abele, S. Baeßler, B. Märkisch, M. Schumann, T. Soldner, and O. Zimmer, Nuclear Instruments and Methods in Physics Research Section A: Accelerators, Spectrometers, Detectors and Associated Equipment **596**, 238 (2008).
[15] L. Hayen, Phys. Rev. D **103**, 113001 (2021), arXiv:2010.07262 [hep-ph] .
[16] M. Gorchtein and C.-Y. Seng, JHEP **10**, 053 (2021), arXiv:2106.09185 [hep-ph] .
[17] A. Sirlin, Phys. Rev. **164**, 1767 (1967).
[18] A. Sirlin, Rev. Mod. Phys. **50**, 573 (1978), [Erratum: Rev.Mod.Phys. 50, 905 (1978)].
[19] N. Carrasco, V. Lubicz, G. Martinelli, C. T. Sachrajda, N. Tantalo, C. Tarantino, and M. Testa, Phys. Rev. D **91**, 074506 (2015), arXiv:1502.00257 [hep-lat] .
[20] D. Giusti, V. Lubicz, G. Martinelli, C. T. Sachrajda, F. Sanfilippo, S. Simula, N. Tantalo, and C. Tarantino, Phys. Rev. Lett. **120**, 072001 (2018), arXiv:1711.06537 [hep-lat] .
[21] Y. Aoki et al., (2021), arXiv:2111.09849 [hep-lat] .
[22] A. Walker-Loud et al., PoS **CD2018**, 020 (2020), arXiv:1912.08321 [hep-lat] .
[23] B. Märkisch et al., Phys. Rev. Lett. **122**, 242501 (2019), arXiv:1812.04666 [nucl-ex] .
[24] S. Ando, H. W. Fearing, V. P. Gudkov, K. Kubodera, F. Myhrer, S. Nakamura, and T. Sato, Phys. Lett. B **595**, 250 (2004), arXiv:nucl-th/0402100 .
[25] A. Falkowski, M. González-Alonso, A. Palavrić, and A. Rodríguez-Sánchez, (2021), arXiv:2112.07688 [hep-ph] .
[26] J. Gasser and H. Leutwyler, Annals Phys. **158**, 142 (1984).
[27] J. Gasser and H. Leutwyler, Nucl. Phys. B **250**, 465 (1985).
[28] E. E. Jenkins and A. V. Manohar, Phys. Lett. B **255**, 558 (1991).
[29] U.-G. Meißner and S. Steininger, Phys. Lett. B **419**, 403 (1998), arXiv:hep-ph/9709453 .
[30] G. Muller and U.-G. Meißner, Nucl. Phys. B **556**, 265 (1999), arXiv:hep-ph/9903375 .
[31] J. Gasser, M. A. Ivanov, E. Lipartia, M. Mojzis, and A. Rusetsky, Eur. Phys. J. C **26**, 13 (2002), arXiv:hep-ph/0206068 .
[32] M. Knecht, H. Neufeld, H. Rupertsberger, and P. Talavera, Eur. Phys. J. C **12**, 469 (2000), arXiv:hep-ph/9909284 .
[33] S. Weinberg, Physica A **96**, 327 (1979).
[34] S. Weinberg, Phys. Lett. B **251**, 288 (1990).
[35] S. Weinberg, Nucl. Phys. B **363**, 3 (1991).
[36] R. E. Behrends and A. Sirlin, Phys. Rev. Lett. **4**, 186 (1960).
[37] M. Ademollo and R. Gatto, Phys. Rev. Lett. **13**, 264 (1964).
[38] V. Bernard, N. Kaiser, J. Kambor, and U.-G. Meißner, Nucl. Phys. B **388**, 315 (1992).
[39] J. Kambor and M. Mojzis, JHEP **04**, 031 (1999), arXiv:hep-ph/9901235 .
[40] V. Bernard and U.-G. Meißner, Phys. Lett. B **639**, 278 (2006), arXiv:hep-lat/0605010 .
[41] A. Czarnecki, W. J. Marciano, and A. Sirlin, Phys. Rev. D **70**, 093006 (2004), arXiv:hep-ph/0406324 .
[42] R. Gupta, Y.-C. Jang, B. Yoon, H.-W. Lin, V. Cirigliano, and T. Bhattacharya, Phys. Rev. D **98**, 034503 (2018), arXiv:1806.09006 [hep-lat] .
[43] M. Hoferichter, J. Ruiz de Elvira, B. Kubis, and U.-G. Meißner, Phys. Rept. **625**, 1 (2016), arXiv:1510.06039 [hep-ph] .
[44] D. Siemens, J. Ruiz de Elvira, E. Epelbaum, M. Hoferichter, H. Krebs, B. Kubis, and U.-G. Meißner, Phys. Lett. B **770**, 27 (2017), arXiv:1610.08978 [nucl-th] .

[45] M. A. P. Brown et al. (UCNA), Phys. Rev. C **97**, 035505 (2018), arXiv:1712.00884 [nucl-ex] .

[46] O. Naviliat-Cuncic and N. Severijns, Phys. Rev. Lett. **102**, 142302 (2009), arXiv:0809.0994 [nucl-ex] .

[47] M. Gorchtein, Physical Review Letters **123**, 042503 (2019), arXiv:1812.04229 .

[48] M. Di Carlo, G. Martinelli, D. Giusti, V. Lubicz, C. T. Sachrajda, F. Sanfilippo, S. Simula, and N. Tantalo, PoS **LATTICE2019**, 196 (2019), arXiv:1911.00938 [hep-lat] .

[49] M. G. Endres, A. Shindler, B. C. Tiburzi, and A. Walker-Loud, Phys. Rev. Lett. **117**, 072002 (2016), arXiv:1507.08916 [hep-lat] .

[50] S. R. Coleman, J. Wess, and B. Zumino, Phys. Rev. **177**, 2239 (1969).

[51] C. G. Callan, Jr., S. R. Coleman, J. Wess, and B. Zumino, Phys. Rev. **177**, 2247 (1969).

[52] V. Bernard, N. Kaiser, and U.-G. Meißner, Int. J. Mod. Phys. E **4**, 193 (1995), arXiv:hep-ph/9501384 .

[53] V. P. Gudkov, G. L. Greene, and J. R. Calarco, Phys. Rev. C **73**, 035501 (2006), arXiv:nucl-th/0510012 .

[54] S.-i. Ando, J. A. McGovern, and T. Sato, Phys. Lett. B **677**, 109 (2009), arXiv:0902.1194 [nucl-th] .